Biosensors and Bioelectronics 40 (2013) 227–232

Contents lists available at SciVerse ScienceDirect

Biosensors and Bioelectronics

journal homepage: www.elsevier.com/locate/bios

Capacitive immunoaffinity biosensor based on vertically paired ring-electrodes

Ga-Yeon Lee [a], Yong-Hwan Choi [a], Ha-Wook Chung [a], Hyuk Ko [a], Sungbo Cho [b], Jae-Chul Pyun [a,*]

[a] Department of Materials Science and Engineering, Yonsei University, 50 Yonsei-Ro, Seodaemun-Gu Seoul 120-749, Korea
[b] Department of Biomedical Engineering, Gachon University, Inchon 406-799, Korea

ARTICLE INFO

Available online 16 August 2012

Keywords:
Capacitive
Immunoassay
Non-labeled detection
Parylene-C
Impedance

ABSTRACT

A capacitive biosensor was developed by using a vertically paired ring-electrode for the non-labeled immunoassay. The vertically paired ring-electrode was prepared by sequential deposition and etching processes. Two electrodes were layered on glass substrate by sputtering of gold layers with thicknesses of 50 nm and 100 nm, and a parylene-C film with a thickness of 550 nm was positioned between the electrode layers as a dielectric material by thermal deposition. The top layer was made by spin coating of SU-8. And then, the ring-electrodes were exposed at the wall of the layered structure by sequential etching processes. The fabricated electrodes were characterized by cyclic voltammetry of a well-known redox couple of 3,3',5,5'-tetramethylbenzidine. The non-labeled detection of antigen–antibody interaction was demonstrated by using anti-horseradish peroxidase (HRP) antibodies and C-reactive protein (CRP) as model analytes. When the model analytes were bound to the vertically paired ring-electrode, the impedance change was measured during the immunoassay steps, and the measured impedance was analyzed by using a model circuit of the ring-electrode, and the capacitance was estimated to be dependent on the adsorption of analytes between the ring-electrodes.

1. Introduction

Immunoaffinity biosensors have been developed by using the highly sensitive antigen–antibody interaction for the detection of a target analyte in complex mixtures. Usually, the non-labeled detection of immunoaffinity biosensors could be achieved by using various kinds of transducers, such as electrochemical (Mirsky et al., 1997), surface plasmon resosnance (Horan et al., 1999; Lahiri et al., 1999; Ostuni et al., 1999; Shin et al., 2010), mass sensitive (Pyun et al., 1998), and so on. Among the transducers, capacitive biosensors have been interested for non-labeled detection of antigen–antibody interactions because of the high sensitivity and the relatively simple instrumentation and so on (Berggren et al., 1998, 1999, 2001; Dijksma et al., 2001; Bard and Faulkner, 2001; Bart et al., 2005; Carrara et al., 2009a,b; Kang et al., 2010). The capacitance is determined by the equation: $C=\varepsilon \cdot A/d$, where C, ε, A, d represent capacitance, permittivity constant, area of electrode, distance between electrodes, respectively. The idea of this work is to fabricate the capacitive biosensor by using vertically positioned electrodes. In order to increase the sensitivity the distance between electrodes was minimized by using a thin parylene film as a dielectric layer. For the capacitive biosensors, many approaches have been taken in the design of interdigitated electrodes (IDEs). The IDE-type electrodes consist of comb-shaped electrodes facing each other, which are electrically separated with a micro- or nano-gap structure. Nano-gap IDEs enable to measure label-free biomolecular interactions such as DNA hybridization and antigen–antibody reactions (Yi et al., 2005; Kim et al., 2009; Zou et al., 2007). Usually, such IDE-type electrodes with the distance between electrodes of less than 1 μm have been fabricated by using costly and time-consuming processes such as E-beam lithography (Zou et al., 2007), focused ion-beam fabrication (Santschi et al., 2006), and a mass-producible submicron-gap IDE via a stepper photolithography (Ahn et al., 2011). In this work, a new type of vertically paired ring-electrode was fabricateded for the non-labeled immunoassay by using the parylene-C film with a thickness of less than 1 μm as a dielectric layer. In order to demonstrate the non-labeled immunoassay, two kinds of model analytes of anti-horseradish peroxidase (HRP) antibodies and C-reactive protein (CRP) were used with the vertically paired ring-electrodes. When the model analytes were bound to the vertically paired ring-electrode, the impedance change was measured during the immunoassay steps, and the measured impedance was analyzed by using a model circuit of the ring-electrode. From the model circuit analysis, the impedance between the ring-electrodes was calculated to be largely dependent on the capacitance change of the protein layer positioned at the current pathway. Therefore, the non-labeled detection of the target

* Corresponding author. Tel.: +02 2123 5851; fax: +02 365 5882.
E-mail address: jcpyun@yonsei.ac.kr (J.-C. Pyun).

0956-5663/$ - see front matter © 2012 Elsevier B.V. All rights reserved.
http://dx.doi.org/10.1016/j.bios.2012.07.028

analyte bound to the antibodies immobilized on the wall of the ring-electrode could be achieved.

Here, the fabrication of ring-electrode was presented by controlling the thickness of parylene-C film with quartz crystal microbalance (QCM), and the fabricated electrode was characterized by using a well-known redox couple of 3,3',5,5'-tetramethylbenzidine. The non-labeled detection of antigen–antibody interaction was demonstrated by using horseradish peroxidase (HRP) and C-reactive protein (CRP) as model analytes. The impedance was analyzed by using a model circuit of the ring-electrode, and the non-labeled detection of antigen–antibody interaction was demonstrated by estimation of capacitance change during the immunoassay steps.

2. Materials and methods

2.1. Materials

C-reactive protein (CRP), anti-CRP antibodies were purchased from AbCam (Cambridge, UK). Horseradish peroxidase (HRP), anti-HRP antibody, 3,3',5,5'-tetramethylbenzidine (TMB) and other chemicals of analytical grade were purchased from Sigma-Aldrich Korea (Seoul, Korea).

2.2. Fabrication of nano-gap-ring electrode

The vertically paired ring-electrode was prepared on a glass substrate by a sequential deposition of gold electrode (100 nm), parylene-C film (550 nm), gold electrode (50 nm), SU-8 layer (1.7 μm). Two gold layers were sputtered with a thickness of 100 nm by using a metal mask with a square-shaped opening (10×10 mm^2), and the square-shaped superimposed area was designed to be 5×5 mm^2 as shown in Fig. 1. Between the gold layers, parylene-C (Femto Science Co., Korea) film with a thickness of 550 nm was thermally deposited by the following polymerization steps: (1) evaporation of parylene dimers at the temperature of 160 °C, (2) pyrolysis for the production of highly reactive p-xylene radical at the temperature of 650 °C, and (3) deposition on the gold layer at room temperature (Jeon et al., 2010, 2011). The whole coating procedure was reproducibly carried out by using a microprocessor-controlled parylene coater from Femto Science Co (Korea). After the parylene-C dimer was completely evaporated, the deposition was carried out by supplying the evaporated parylene-C monomer gas into the deposition chamber under vacuum condition of less than 5 Pa at room temperature. For the monitoring of parylene-C deposition, the QCM response was measured from the beginning of evaporation step, and the mass changings on the QCM sensor from the deposition of a parylene film were converted into the frequency shift based on the Sauerbrey equation: $\Delta f = -2\Delta m f_0^2 / [A(\mu_q \rho_q)^{1/2}]$, where ρ_q is the quartz density, μ_q is the crystal shear module, f_0 is the crystal fundamental frequency, A is the piezoelectrically active area of crystal (defined by the area of the deposited metallic film on the crystal), and Δm and Δf correspond to mass and system frequency changes, respectively (Ansorena et al., 2011; Harbecka et al., 2011). For the thickness control of parylene-C film, the QCM response was measured from the beginning of evaporation step, and the thermal deposition was finished when the QCM frequency shift reached to the value corresponding to the targeted thickness of the parylene film-C. As a top layer, the SU-8 coating (1.7 μm) was made on the gold layer as a protective layer by the spin-coating. The hole-shaped area with a diameter of 2 mm was exposed to UV light for the etching process, and then the SU-8 layer was baked at 110 °C.

The ring-electrodes were exposed by the sequential etching processes as shown in Fig. 1. The hole-shaped opening with a diameter of 2 mm was made at the superposed area of gold layers. The ring-electrodes were exposed by a series of etching process. As the first step, the SU-8 layer was etched by dipping in a commercial developer (Micro Chem, USA). The gold layer was etched by dipping in 1% ferricyanide solution with 1% NaCN for 30 s at room temperature (Utaka et al., 2007). The parylene film was etched by LF-plasma treatment with a power of 10 W for 1 h (Jeon et al., 2010, 2011). The second gold layer on the glass substrate was also etched by dipping in 1% ferricyanide solution with 1% NaCN for 1 min at room temperature.

2.3. Electrochemical measurements

The cyclic voltammetry (CV) was performed by using a potentiostat from IVIUM Technologies (Compactstat, Netherlands). For the characterization of the ring-electrodes, three-electrode system was prepared by using the ring-electrode as a working electrode. An external reference electrode of Ag/AgCl and a counter electrode made of Pt-wire were used for the analysis of a well-known redox couple of 3,3',5,5'-tetramethylbenzidien (TMB). The cyclic voltammogram (CV) of TMB sample was obtained at the potential range from −400 mV to +600 mV (versus Ag/AgCl) at the scanning rate of 30 mV/s. The TMB solution was prepared to be 0.02 mg/ml in 100 mM sodium citrate buffer at pH 5.0 with 0.2% hydrogen peroxide.

The impedance measurement was also performed by using the potentiostat from IVIUM Technologies (Compactstat, Netherlands), and two ring-electrodes were used for the impedance measurement at the frequency range from 100 Hz to 100 kHz with an applied potential of 10 mV. The measured impedance of the electrode sensor was analyzed by using an equivalent circuit model which consists of the interfacial electrode impedance consisted of the constant phase

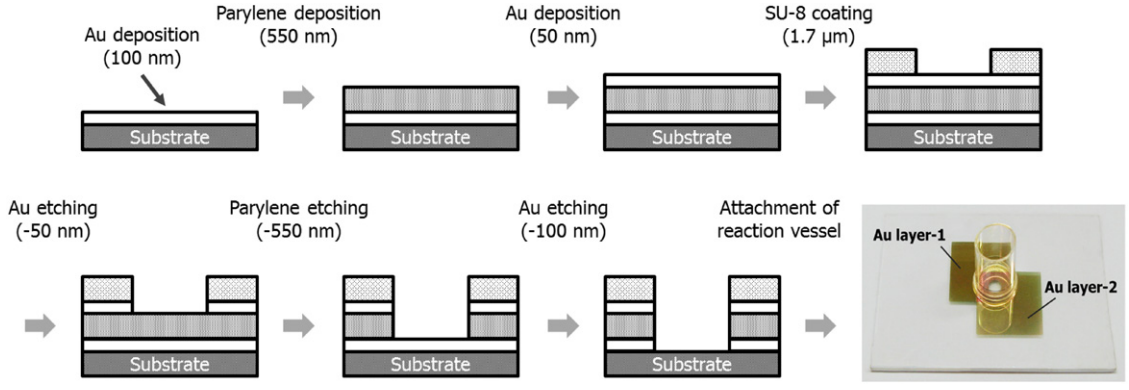

Fig. 1. Fabrication process of vertically paired ring-electrode. The electrode was prepared by a sequence of deposition processes and a series of etching processes.

element (CPE_{el}), and a series medium resistance (R_s) with a parallel stray capacitance ($C_{Parylene}$) (Cho and Thielecke, 2007).

3. Results and discussion

3.1. Characterization of vertically paired ring-electrode

The vertically paired ring-electrode was prepared by a sequential deposition process and a series of etching process as shown in Fig. 1. From the sequential deposition process, the following layers were made on a glass substrate: gold electrode (100 nm, counter electrode), parylene film (550 nm, dielectric layer), gold electrode (50 nm, working electrode), Su-8 layer (1.7 μm, protective layer). The electrodes were exposed by a series of etching process such as SU-8 etching by a commercial developer, gold etching by ferricyanide solution, parylene film etching by plasma treatment.

The morphological change during the etching process was monitored by using AFM analysis. As shown in Fig. 2, the thickness of etched layer was estimated to be SU-8 layer (500 nm, protective layer), the first etched gold electrode (50 nm), parylene-C film (550 nm, dielectric layer), the second gold electrode (100 nm) from the AFM images. The etched edge of electrode was observed to be nearly a vertically walled structure with a slope with an angle of 80°. From the AFM image, the protective layer of SU-8 was considered to be also etched during etching process of the parylene-C film by plasma treatment, and the final thickness was estimated to be approximately 550 nm. On the top layer, the cylindrical tubing for immunoassays was attached to the SU-8 surface.

The parylene-C film was thermally deposited as a dielectric layer between the gold layers (Kang et al., 2010; Kim et al., 2009). As the parylene-C film was made by the thermal decomposition of parylene dimer (p-xylylene) at 650 °C, the thickness control was required at the thickness range of a few hundred nanometers. In this work, the thickness control was carried out by using a quartz crystal microbalance (QCM) at the deposition chamber. As shown in Fig. 3, the resonance frequency shift of QCM was correlated to the thickness of parylene-C film from the AFM analysis. By using the QCM monitoring method, the parylene-C film at the thickness range of less than 100 nm could be controlled with a linearity factor of 0.96 ($n=11$) as shown in Fig. 3. In this work, the parylene film deposition was fixed to be 500 nm thick for the immunoassays, and the thickness was analyzed to be 550 ± 50 nm ($n=5$).

The ring-electrodes exposed by the series of etching processes was tested by cyclic voltammetry of 3,3',5,5'-tetramethylbenzidine (TMB) as a model redox couple (Pyun et al., 2005). TMB has been used as a chromogenic substrate of horseradish peroxidase (HRP) which is usually labeled to the reporting antibodies of immunoassays. The TMB molecule is oxidized by HRP, and the color of TMB turns to blue (1st oxidation, $\lambda_{max}=650$) and yellow (2nd oxidation, $\lambda_{max}=450$) by two oxidation steps. For the cyclic voltammetry, 3-electrode system was used with an external reference electrode of Ag/AgCl and a counter electrode made of Pt-wire. As shown in Fig. 4, two oxidation steps were separately observed in the cyclic voltammogram. As the 1st oxidation product of TMB turns into the 2nd oxidation product of TMB at an acidic condition, the cyclic voltammogram after treatment of 1 M sulfuric acid (equivalent volume) usually shows only a single peak of 2nd oxidation product of TMB. Such a step-shaped graph as shown in Fig. 4 is well-known for the microelectrodes, and LOD (limit of detection) could be improved by clear determination of electrochemical oxidative and reductive peaks. Usually, microelectrodes induce hemispherical diffusion profiles and they show improved mass transfer compared to that of macro-sized

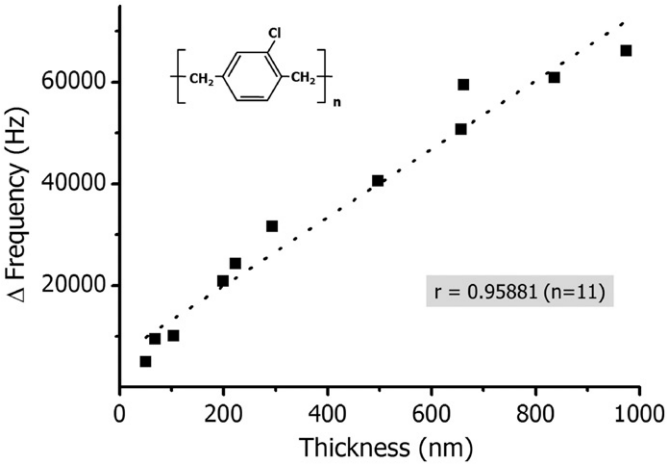

Fig. 3. Correlation curve of parylene-C film deposition between the QCM response and the thickness of parylene-C film from AFM analysis (n=11).

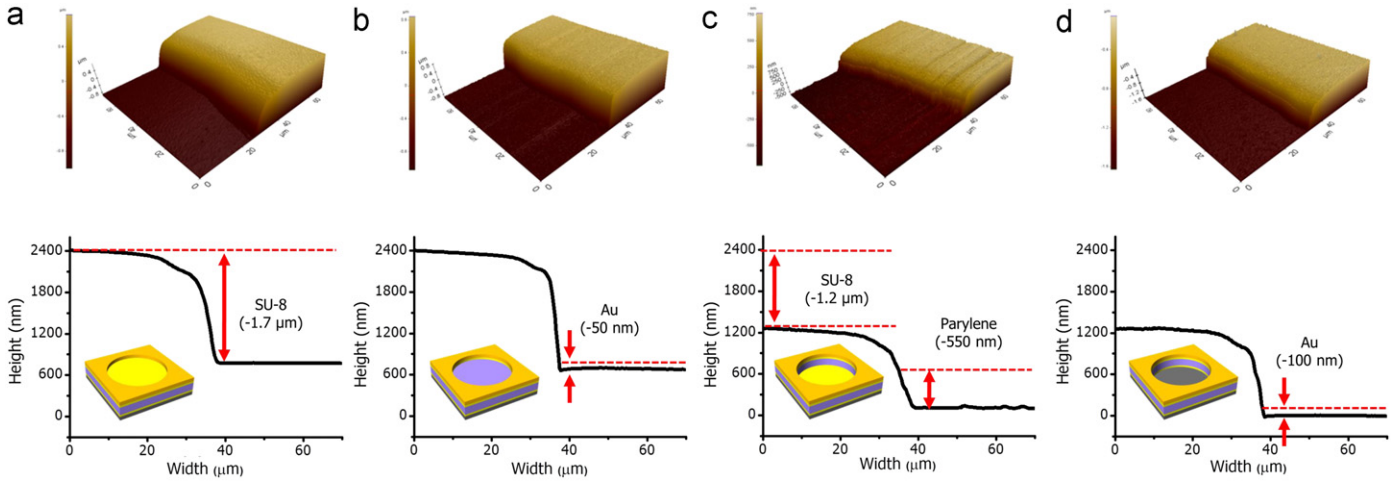

Fig. 2. AFM images of ring-electrode in a series of etching processes. (a) SU-8 etching (1.7 μm, protective layer) by developer treatment, (b) the first gold layer (50 nm) etching by using the ferricyanide based gold etcher, (c) parylene-C film (550 nm) etching by plasma treatment and (d) the second gold layer (100 nm) etching.

electrodes. Such a diffusion profile brings much higher current density which translates into a high signal to noise ratio (Kim et al., 2009). These results show that the fabricated ring-electrodes could be used as a working electrode which can perform redox-reaction of TMB molecule.

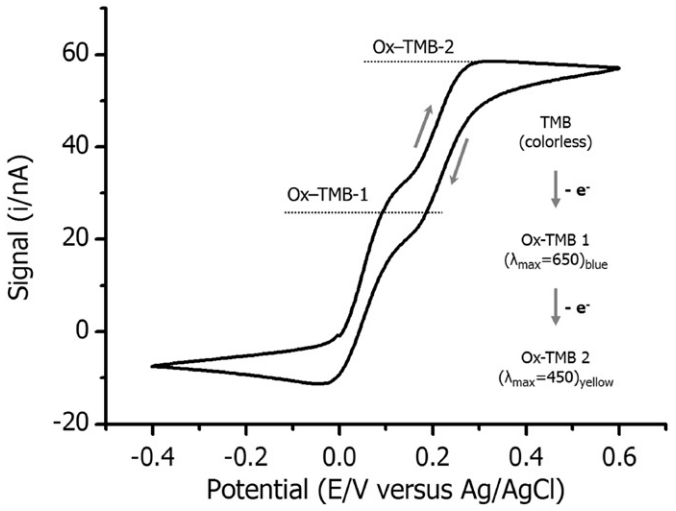

Fig. 4. Cyclic voltammetric analysis of 3,3',5,5'-tetramethylbenzidine (TMB) by using a ring-electrode as a working electrode. The cyclic voltammogram (CV) of TMB sample was obtained at the potential range from −400 mV to +600 mV (versus Ag/AgCl) at the scanning rate of 30 m.

3.2. Immunoassay with vertically paired ring-electrode

For the demonstration of immunoassays with the vertically paired ring-electrode, anti-HRP antibodies and C-reactive protein were used as model analytes. For the analysis of anti-HRP antibodies as a target analyte, the HRP was immobilized on the electrode by physical adsorption. And then, a series of standard samples with known concentrations of anti-HRP antibodies were injected to the ring-electrode. Between the sample injections, the electrode was rinsed by using the washing solution. After washing step, the impedance was measured at the frequency range between 100 Hz and 1 MHz at the applied potential of 10 mV as shown in Fig. 5(a). The measured impedance of the electrode sensor was analyzed by using an equivalent circuit model which consists of the constant phase element (CPE_{el}), and a series medium resistance (R_s) with a parallel stray capacitance ($C_{Parylene}$) (Cho and Thielecke, 2007).

The values of the parameters were extrapolated to minimize the sum of the squared deviations between the equivalent model and the measured impedance spectra by nonlinear-curve-fitting (Cho and Thielecke, 2007). As the parylene is a high insulating material, the current flows through the exposed electrodes at low frequency. As the surface area (6.3×10^{-4} mm^2) of the ring-electrode is quite small, the impedance at the electrode interface with solution is considered to be quite high. Thus total impedance is mostly contributed by the interfacial electrode impedance and closely related to the capacitance factor in the imaginary part of the total impedance. As shown in Fig. 5(b), the capacitance according to the frequency was estimated during each step of

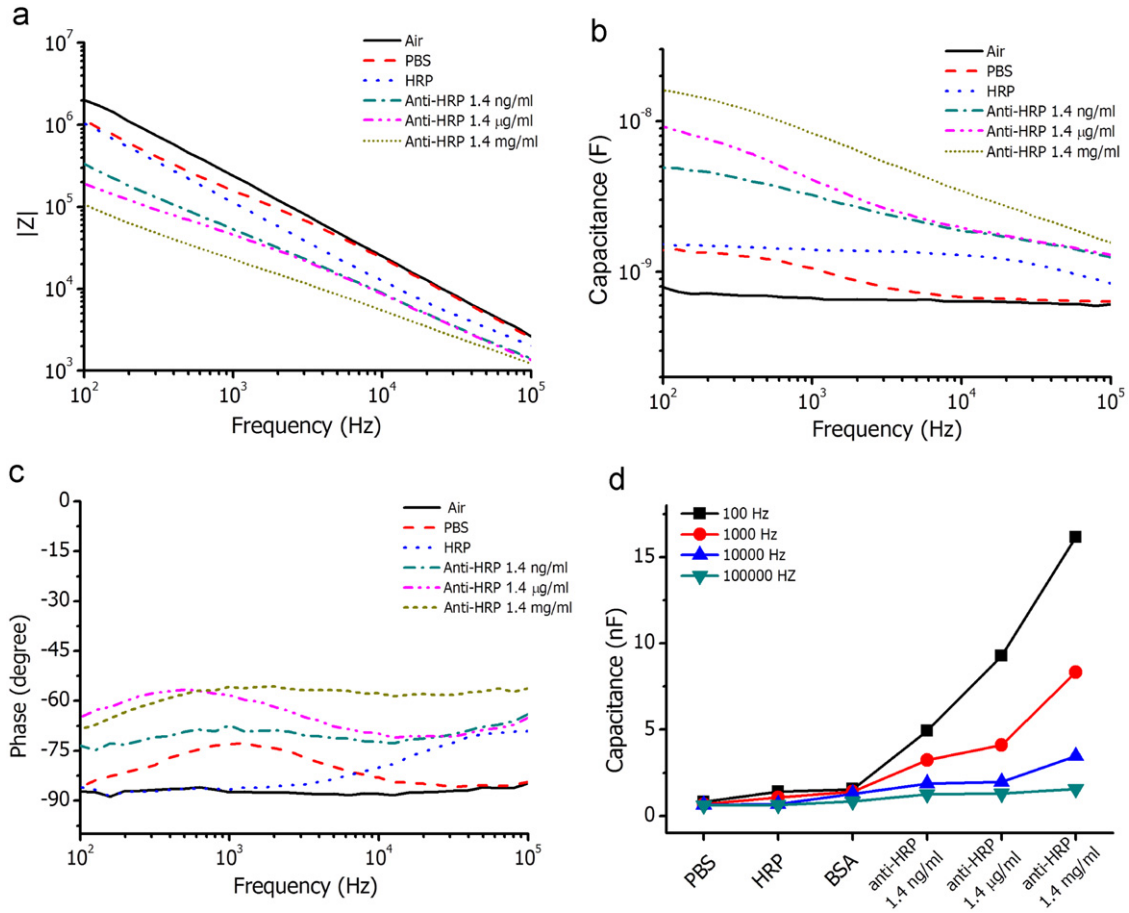

Fig. 5. Impedance analysis during the immunoassay of anti-HRP antibodies. (a) Measured impedance according to the applied frequency from the ring-electrode, (b) capacitance part of imaginary part of total impedance calculated from the model circuit, (c) phase change during the immunoassay and (d) capacitance value according to the applied frequency during the immunoassay steps.

the immunoassay, and the change of capacitance was observed at low frequency range of the impedance spectrum as in the case of the double layer capacitance of IDE electrode (Yang et al., 2004). The phase of the vertically paired ring-electrode in air was close to −90° in the frequency range of 100 Hz–100 kHz, meaning that the impedance spectra were contributed by the capacitive reactance. With the application of Anti-HRP into the HRP treated-electrode system, the phase was increased and the relative magnitude of reactance was decreased as shown in Fig. 5(c). This result indicated that the increase of the capacitance was dependent on the applied concentration of anti-HRP antibodies. When the capacitance was plotted according to the frequency, the capacitance increased according to the amount of adsorbed proteins as shown in Fig. 5(d). These results show that the vertically paired ring-electrode can be used for the quantitative analysis of adsorbed proteins without additional labeling process.

The vertically paired ring-electrode was applied for the detection of C-reactive protein (CRP) which was known to be a biomarker of inflammatory diseases such as rheumatoid arthritis (Ko et al., 2011). For this work, the anti-CRP antibodies were immobilized at the well of the ring-electrode, and then the standard curve was prepared by analyzing a series of standard samples with known concentrations of CRP. As shown in Fig. 6(a), the impedance plot was obtained according to the applied frequency at the range from 100 Hz to 100 kHz. By using the same model circuit, the capacitance factor was calculated from the imaginary part of the measured impedance as shown in Fig. 6(b). In this case, the change in capacitance by the binding of CRP to the anti-CRP antibodies was observed to be increased at the low frequency range. Compared to the phase in air, the value measured when CRP was applied to the anti-CRP modified-electrode system was increased as shown in Fig. 6(c). It was also observed that the capacitive reactance was decreased or the capacitance was increased in dependency on the concentration of CRP. As shown in Fig. 6(d), the change in capacitance was plotted at each step of the immunoassay for CRP. In this plot, the change in capacitance was clearly observed to be increased as the applied frequency was lowered from 100 KHz to 100 Hz. These results shows that the vertically paired ring-electrode can be also applied for the detection of proteins at the size of 120–140 kDa by immunoassays.

4. Conclusions

A vertically paired ring-electrode was developed for the non-labeled immunoassay. The vertically paired ring-electrode was prepared by sequential deposition and etching processes. Two electrodes were layered on glass substrate by sputtering of gold layers with a thickness of 50 nm, and a parylene-C film with a thickness of 550 nm was positioned between the electrode layers as a dielectric material by thermal deposition. The top layer was made by spin coating of SU-8. And then, the ring-electrodes were exposed at the wall of the layered structure by sequential etching processes. From the sequential deposition process, the following layers were made on a glass substrate: gold electrode (100 nm,

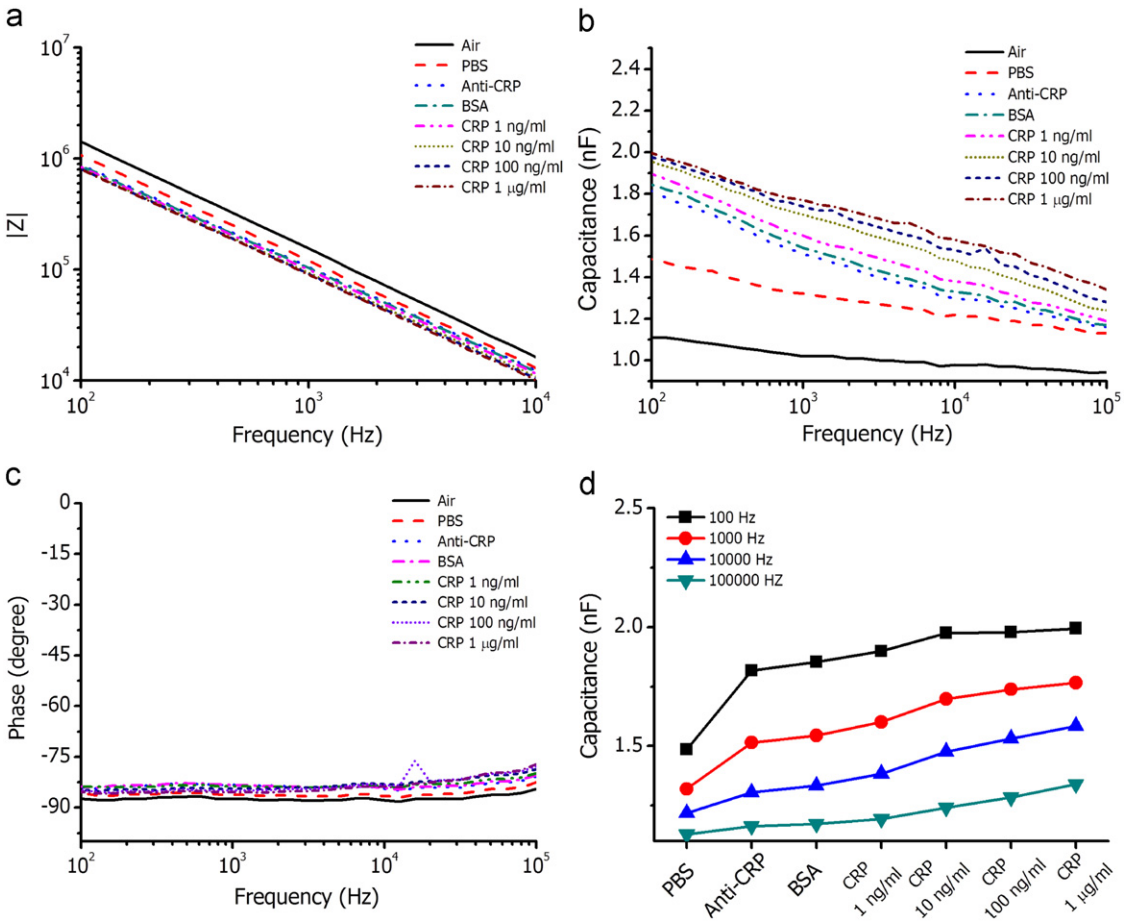

Fig. 6. Impedance analysis during the immunoassay of C-reactive protein (CRP). (a) Impedance measurements according to the applied frequency from the ring-electrode, (b) capacitance part of imaginary part of total impedance calculated from the model circuit, (c) phase change during the immunoassay and (d) capacitance value according to the applied frequency during the immunoassay steps.

counter electrode), parylene film (550 nm, dielectric layer), gold electrode (50 nm, working electrode), Su-8 layer (1.7 μm, protective layer). The fabricated electrodes were characterized by cyclic voltammetry of a well-known redox couple of 3,3',5,5'-tetramethylbenzidine. The cyclic voltammogram showed a typical result from the microelectrode and two oxidation steps could be separately observed. These results show that the fabricated ring-electrodes could be used as a working electrode which can perform redox-reaction of TMB molecule. The non-labeled detection of antigen–antibody interaction was demonstrated by using anti-horseradish peroxidase (HRP) antibodies and C-reactive protein (CRP) as model analytes. When the model analytes were bound to the vertically paired ring-electrode, the impedance change was measured during the immunoassay steps at the frequency range between 100 Hz and 100 kHz at the applied potential of 10 mV. The measured impedance of the electrode sensor was analyzed by using an equivalent circuit model which consists of the constant phase element (CPE_{el}), and a series medium resistance (R_s) with a parallel stray capacitance ($C_{Parylene}$). From the analysis by using a model circuit of the ring-electrode, and the capacitance was estimated to be dependent on the adsorption of analytes between the ring-electrodes. From these results, the vertically paired ring-electrode was tested to be feasible for the non-labeled detection of proteins.

Acknowledgments

This work was supported by DAPA and ADD. This research was also supported by the National Research Foundation of Korea (NRF) funded by the Ministry of Education, Science and Technology (2009-0082188, 2009-008-1529, 2010-0020772 and 2011-0020285).

References

Ahn, J.h., Ahn, T.H., Lee, T.H., Li, K.H., Hong, S.H., Ko, J.H., Kim, Y.S., Shin, Y.B., Kim, M.G., 2011. Biosensors and Bioelectronics 26, 4690–4696.
Ansorena, P., Zuzuarreguia, A., Perez-Lorenzoa, E., Mujikab, M., Arana, S., 2011. Sensors and Actuators B 155, 667–672.
Bard, A.J., Faulkner, L.R., 2001. Electrochemical Methods, 2nd ed. John Wiley and sons Ltd., New York.
Bart, M., Stigter, E.C.A., Stapert, H.R., de Jong, G.J., van Bennekom, W.P., 2005. Biosensors and Bioelectronics 21, 49.
Berggren, C., Bjarnason, B., Johansson, G., 1998. Biosensors and Bioelectronics 13, 1061.
Berggren, C., Stalhandske, P., Brundell, J., Johansson, G., 1999. Electroanalysis 11, 156.
Berggren, C., Bjarnason, B., Johansson, G., 2001. Electroanalysis 13, 173.
Carrara, S., Bhalla, V., Stagni, C., Benini, L., Ferretti, A., Valle, F., Gallotta, A., Ricco, B., Samori, B., 2009a. Sensors and Actuators B: Chemical 136, 163–172.
Carrara, S., Benini, L., Bhalla, V., Stagni, C., Ferretti, A., Cavallini, A., Gallotta, A., Ricco, B., Samori, B., 2009b. Biosensors and Bioelectronics 24, 3425–3429.
Cho, S.B., Thielecke, H., 2007. Biosensors and Bioelectronics 22, 1764–1768.
Dijksma, M., Kamp, B., Hoogvliet, J.C., van Bennekom, W.P., 2001. Analytical Chemistry 73, 901.
Harbecka, M., Dilek, Erbahara, D., Gurola, I., Musluoglua, E., Ahsena, V., Ozturk, Z.Z., 2011. Sensors and Actuators B 155, 298–303.
Horan, N., Yan, L., Isobe, H., Whitesides, G.M., Kahne, D., 1999. Proceedings of the National Academy of Sciences 21, 11782–11786.
Jeon, B.J., Kim, M.H., Pyun, J.C., 2011. Sensors and Actuators B 154, 89–95.
Jeon, B.J., Kim, M.H., Pyun, J.C., 2010. Journal of Immunological Methods 353, 44–48.
Kang, B.K., Yeo, U.J., Yoo, K.H., 2010. Biosensors and Bioelectronics 25, 1592–1596.
Kim, J.I., Bordeanu, A., Pyun, J.C., 2009. Biosensors and Bioelectronics 24, 1394–1398.
Kim, Y.S., Niazi, J.H., Gu, M.B., 2009. Analytica Chimica Acta 634, 250–254.
Ko, H., Lee, G.Y., Jin, B.J., Pyun, J.C., 2011. Biochip Journal 5, 242–245.
Lahiri, J., Issac, L., Tien, J., Whitesides, G.M., 1999. Analytical Chemistry 71, 777–790.
Mirsky, V.M., Riepl, M., Wolfbeis, O.S., 1997. Biosensor and Bioelectronics 68, 1.
Ostuni, E., Yan, L., Whitesides, G.M., 1999. Colloids and Surfaces B: Biointerfaces 15, 3–30.
Pyun, J.C., Beutel, H., Meyer, J.U., Ruf, H.H., 1998. Biosensors and Bioelectronics 13, 839–845.
Pyun, J.C., Kim, S.D., Chung, J.W., 2005. Sensors and Actuators B 111-112, 416–422.
Santschi, C., Jenke, M., Hoffmann, P., Brugger, J., 2006. Nanotechnology 17, 2722–2729.
Shin, Y.B., Kim, H.M., Jung, Y.W., Chung, B.H., 2010. Sensors and Actuators B: Chemical 150, 1–6.
Utaka, K., Komatsu, T., Nagano, H., 2007. International Corrosion Engineering Conference. 20–24May.
Yang, L., Li, Y., Griffis, C.L., Johnson, M.G., 2004. Biosensors and Bioelectronics 24, 3425–3429.
Yi, M., Jeong, K.H., Lee, L.P., 2005. Biosensors and Bioelectronics 20, 1320–1326.
Zou, Z., Kai, J., Rust, M.J., Han, J., Ahn, C.H., 2007. Sensor and Actuators A: Physics 136, 518–526.